Physica 11D (1984) 1–24
North-Holland, Amsterdam

NONLOCAL MAPS

M.V. BERRY, J.O. INDEKEU* and M. TABOR†
H.H. Wills Physics Laboratory, Tyndall Avenue, Bristol BS8 1TL, UK

and

N.L. BALAZS
State University of New York at Stony Brook, N.Y. 11790, USA

Received 4 April 1983
Revised 12 October 1983

A new kind of area-preserving map of the phase plane is introduced to represent the dynamics of interacting particles on a line. Unlike the familiar point map, the map is nonlocal in the sense that the evolution of a point in the phase plane depends not only on its position but also on the positions of other points, weighted by an evolving phase-plane density.

In the case where this density is uniform and confined within a closed boundary B in the phase plane, the evolution of B is followed for a great variety of interaction potentials. Numerical experiments and analytical arguments show that a simple B develops great complexity. The resulting morphologies, incorporating fission and fusion of particle densities, are illustrated by high resolution graphics.

1. Introduction

Area-preserving maps of the phase plane q, p have been useful in unravelling the complexities of classical Hamiltonian motion for single particles acted on by external forces [1, 2]. An essential feature of these maps is that the state q_{n+1}, p_{n+1} after the nth discrete time step along the particle trajectory depends only on the state q_n, p_n immediately before the nth step. In physical terms, the maps may represent a particle with one freedom moving under a Hamiltonian having time period T, with q and p sampled at multiples of T; or they may represent intersections with the Poincaré surface of section for a particle with two freedoms moving under a stationary Hamiltonian.

Our purpose here is to introduce a new class of area-preserving map which could help in the understanding of *assemblies* of *interacting* particles. Imagine an ensemble representing N particles with mass m, distributed along the line q, by a phase-plane density $\rho(q, p, t)$, where

$$\int\int \mathrm{d}q\, \mathrm{d}p\, \rho(q, p, t) = N. \tag{1.1}$$

(This phase plane is the 2-dimensional 'μ-space' and not the $2N$-dimensional 'Γ-space'.)
The dynamics of the particles is described by the evolution of ρ, which will be considered to take place in discrete time steps with period T, so that we must stipulate how

$$\rho_n(q, p) \equiv \rho(q, p, t = nT) \tag{1.2}$$

evolves to $\rho_{n+1}(q, p)$.

To obtain an explicit map it is convenient to regard the interaction as concentrated into sudden impulses at the end of each time step. Between impulses the phase points move as independent free particles. The impulse on a particle at q from a single particle at q' will be proportional to the derivative of an *interaction potential* $U(q - q')$. At the time $(n + 1)T$ the total impulse at q from the particles in the range q' to $q' + \mathrm{d}q'$ will depend on

* Present address: Institute of Theoretical Physics, Celestijnenlaan 200D, 3030 Leuven, Belgium.

† Present address: La Jolla Institute, P.O. 1434, La Jolla, California 92038, USA.

the configuration particle density at q' which has evolved from $\rho_n(q,p)$ by free motion, i.e. on

$$\int \mathrm{d}p' \rho_n\left(q' - \frac{p'T}{m}, p'\right). \tag{1.3}$$

The complete map from ρ_n to ρ_{n+1} is obtained as

$$\begin{aligned} q_{n+1} &= q_n + \frac{p_n T}{m}, \\ p_{n+1} &= p_n - T \int\int \mathrm{d}q' \, \mathrm{d}p' \rho_n\left(q' - \frac{p'T}{m}, p'\right) \\ &\quad \times U'(q_{n+1} - q'), \\ \rho_{n+1}(q_{n+1}, p_{n+1}) &= \rho_n(q_n, p_n), \end{aligned} \tag{1.4}$$

where U' denotes the first derivative of U. Thus the phase point q_n, p_n moves to q_{n+1}, p_{n+1} under *nonlocal* dynamics determined by the density ρ_n over the whole plane, and the density convects with the phase points as a consequence of conservation of area and particles. Henceforth, T/m and T will be taken as unity, because their values can be trivially absorbed by rescaling p and U. To preserve q-isotropy (parity) U must be an even function. To avoid explosion of the particle density (cf. section 9), $U(0)$ will be taken to be finite.

The nonlocal map (1.4) is much richer in its behaviour than a conventional point map. In essence it is a (generally nonlinear) *field theory* whose infinitely many variables at time n are the values of ρ_n at each phase point q, p. The evolution depends on the whole form of the initial density $\rho_0(q,p)$ as well as on the form of the interaction $U(q-q')$. Many examples will suggest that for most U the evolution is nonintegrable, in the sense that infinitely many conservation laws do not exist, although we have not proved this.

If

$$\rho_0(q,p) = \sum_{i=1}^{N} \delta(q - q_i)\delta(p - p_i), \tag{1.5}$$

the map (1.4) simply gives the full (time-discretized) many-body dynamics of N particles. We shall be interested, however, in cases where ρ_0 is (at least piecewise) a continuous function. Then (1.4) corresponds to a 'Hartree' approximation in which each particle responds to the average field of the others and this paper can be considered as the exploration in detail of a large class of time-dependent one-dimensional Thomas–Fermi problems. In particular, we devote most attention to the case where ρ_0 is constant within some closed boundary curve B_0 and zero outside, and will show (section 2) that (1.4) can be reformulated as a nonlocal map for the evolution of the boundary curve B_n.

The main body of the paper is devoted to a partly analytic but mainly computational survey of how B_n depends on the form of the interaction (attractive or repulsive, short-ranged or long-ranged), as well as on B_0. We shall seek to understand aspects of the *morphogenesis* of B_n as n increases, for instance its growing complexity and near 'fission' in which an all-convex B_0 evolves into two or more 'blobs' connected by a thin filament. In previous studies of the area preserving mappings of curves [3–5], the principal morphologies were 'whorls' and 'tendrils' which developed around elliptic and hyperbolic fixed points of the map; those curves consisted of noninteracting families of classical particles whose interest lay in the fact that they could represent semiclassical quantum states. The nonlocal evolution being studied here does not usually possess fixed points (although Deem and Zubusky [10] exhibit Eulerian fluid vorticity distributions which rotate and translate rigidly), and other morphologies become possible.

In section 3 we make analytical simplifications for the case where the interaction $U(q-q')$ has very long or very short range. Section 4 is devoted to quadratic potentials, for which a complete analytic solution is possible. Section 5 treats the constant-force interaction; section 6 deals with square-well potentials; section 7 is concerned with quartic potentials; section 8 considers Gaussian potentials; section 9 discusses 'interatomic' potentials (attractive at long range, repulsive at short range); section 10 examines sinusoidal potentials.

All these sections are restricted to the case where B_0 (and hence B_n) is a single closed curve. It is interesting to also consider what happens when several such blobs attract each other, and in section 11 we present a (numerical) example of an intertwining so intimate that it is reasonable to speak of 'fusion'.

In section 12 we discuss the question of energy and its conservation for nonlocal maps and their continuous-time limiting cases. This leads naturally to the problem of integrability, which we consider briefly.

In a sense our work is a mechanical and discrete-time analogue of the work of Zabusky [6, 7] on the 'Eulerian' convection of vorticity $\Omega(x, y, t)$ in two-dimensional inviscid incompressible flow, the equations being not (1.4) but

$$\dot{x}(t) = \frac{-1}{2\pi} \iint \mathrm{d}x'\,\mathrm{d}y' \frac{\Omega(x', y', t)(y - y')}{(x - x')^2 + (y - y')^2},$$
$$\dot{y}(t) = \frac{+1}{2\pi} \iint \mathrm{d}x'\,\mathrm{d}y' \frac{\Omega(x', y', t)(x - x')}{(x - x')^2 + (y - y')^2}, \tag{1.6}$$

The symmetry of these equations with respect to x and y has prevented us from discretising time and approximating them as area-preserving maps more closely analogous to (1.4). (It is of course possible to discretize time by conventional predictor–connector algorithms [11], but when this is done area is no longer exactly conserved.)

The absence of external forces on the N particles implies a 'Galilean' redundancy with respect to the initial density $\rho_0(q, p)$, which can easily be derived from (4.1): a density $\rho_0(q - Q_0,\ p - P_0)$, shifted from $\rho_0(q, p)$ by a phase-space translation Q_0, P_0, will evolve exactly as $\rho_0(q, p)$ does, apart from a translation of the whole density by an amount P_0 in the q direction at each iteration. For this reason we need to consider only densities whose phase–space centre of mass lies (and remains) at the origin.

Finally, we note that nonlocal maps are reversible: if in (1.4) T is replaced by $-T$, the orbits of phase points and the evolution of the phase-plane density retrace themselves perfectly (provided the reversal starts by undoing the most recent impulse).

2. Evolution of boundary curves

Let the ensemble representing N particles uniformly populate the interior of a phase-plane curve B_0. If B_0 has area S, (1.1) implies a density

$$\rho_0 = N/S\,. \tag{2.1}$$

Under the nonlocal map, B_0 evolves to B_1, $B_2, \ldots$, but the density remains equal to ρ_0 because area is preserved. Physically, such a step-function density is interesting because it is a model for N interacting Fermions at zero temperature, satisfying the Pauli exclusion principle but otherwise behaving classically.

The development of B_n to B_{n+1} occurs in two stages illustrated in fig. 1. Firstly, the curve B_n is *sheared* in the q direction because of the free motion of the points within it under the first of eqs. (1.4); this results in an intermediate curve which we call $B_{n+1/2}$. Secondly, the curve $B_{n+1/2}$ is *deformed* in the p direction because of the interaction of the points within it under the second of eqs. (1.4); this results in the mapped curve B_{n+1}.

To express B_{n+1} in terms of $B_{n+1/2}$, we first write the second of (1.4), for the step density, as

$$p_{n+1} = p_n - \rho_0 \iint \mathrm{d}q'\,\mathrm{d}p' U'(q_{n+1} - q') \qquad (q', p' \in B_{n+1/2}). \tag{2.2}$$

Now we write the force factor as a divergence in the q', p' plane

$$U'(q_{n+1} - q') = -\nabla_{q',p'} \cdot \{U(q_{n+1} - q')\hat{\boldsymbol{q}}\}, \tag{2.3}$$

where $\hat{\boldsymbol{q}}$ is the unit vector in the q direction. Next, we use the divergence theorem to express the area integral in (2.2) as an integral round $B_{n+1/2}$. If s measures arc length anti-clockwise round the curve (fig. 1) $\tilde{N}(s)$ is the outward normal at s, and $q(s)$

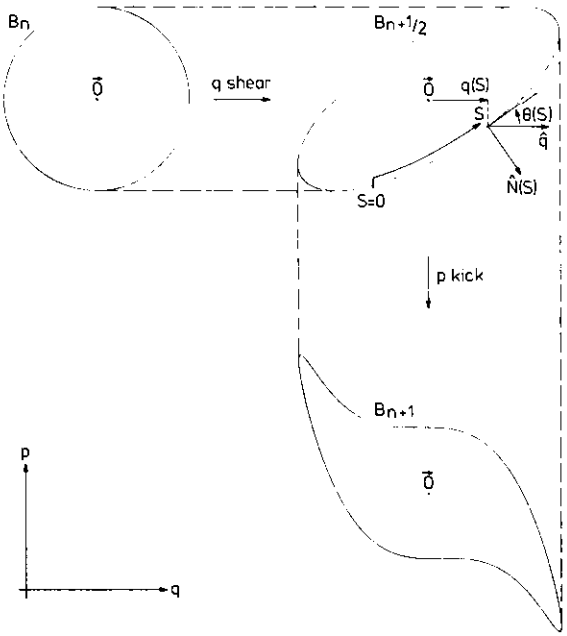

Fig. 1. Two-stage generation of B_{n+1} from B_n.

is the coordinate at s, then

$$\int\int \mathrm{d}q'\,\mathrm{d}p' U'(q_{n+1}-q') = -\oint_{B_{n+1/2}} \mathrm{d}s\, U(q_{n+1}-q(s))\hat{\boldsymbol{q}}\cdot\hat{\boldsymbol{N}}(s) \qquad (q', p' \in B_{n+1/2}). \quad (2.4)$$

Describing $B_{n+1/2}$ by the direction $\theta(s)$ which its anti-clockwise tangent at s makes with $\hat{\boldsymbol{q}}$, we have

$$\hat{\boldsymbol{q}}\cdot\hat{\boldsymbol{N}}(s) = \sin\theta(s). \quad (2.5)$$

Finally, the momentum p_{n+1} of the iterate of the point q_n, p_n on B_n can be written as

$$p_{n+1} = p_n + \rho_0 \oint_{B_{n+1/2}} \mathrm{d}s\, U(q_n + p_n - q(s)) \sin\theta(s). \quad (2.6)$$

This equation clearly shows how each point of B_{n+1} is determined nonlocally by the whole geometry of $B_{n+1/2}$ (which is itself generated by shearing B_n). (It is of course not necessary to consider the rearrangement of the points inside B_n because these preserve the density ρ_0.) Numerical iteration of an initial curve using (2.6) is economical in terms of computer time and forms the basis of computations presented in sections 7–11. Aspects of the numerical methods will be described in appendix A. We emphasize that arc length s is not conserved in these mappings: the lengths of the curves B_n usually increase rapidly with n, rather as they do for point maps (we have confirmed this by many calculations). Even for fixed n, the arc length is not invariant under canonical transformation of the phase plane (although the form of (2.6) is), so that s should be thought of as simply a parameter, without physical meaning.

An important simplification is evident from (2.6). The displacement $p_{n+1} - p_n$ in the p direction, of all the points on and inside $B_{n+1/2}$ which have the same value of $q_{n+1/2}(= q_{n+1} = q_n + p_n)$, is the same. In other words, all p-segments inside $B_{n+1/2}$ move up or down by an amount depending only on q.

The points on the curve B_n for which

$$\mathrm{d}q/\mathrm{d}s = 0\,, \quad \text{i.e. } \cos\theta = 0\,, \tag{2.7}$$

are important because as we shall see they govern the evolution of B for short-ranged potentials. Moreover, they are singularities of the *particle density* which is the projection of ρ onto q,

$$d_n(q) \equiv \rho_0 \int \mathrm{d}p \quad (p = p(q) \in B_n)\,. \tag{2.8}$$

(We remark that the quantity in 1.3 is $d_{n+1}(q')$.) These singularities of projections of *areas* are analogous to the caustics of projection of boundary *curves*, but differ in that their typical form is square-root rather than inverse square-root. We shall therefore call them *anti-caustics* [8]. Fig. 2 illustrates a curve B_n and the corresponding anti-caustics of d_n.

Finally, we point out that in all our numerical simulations we took $\rho_0 = 1$.

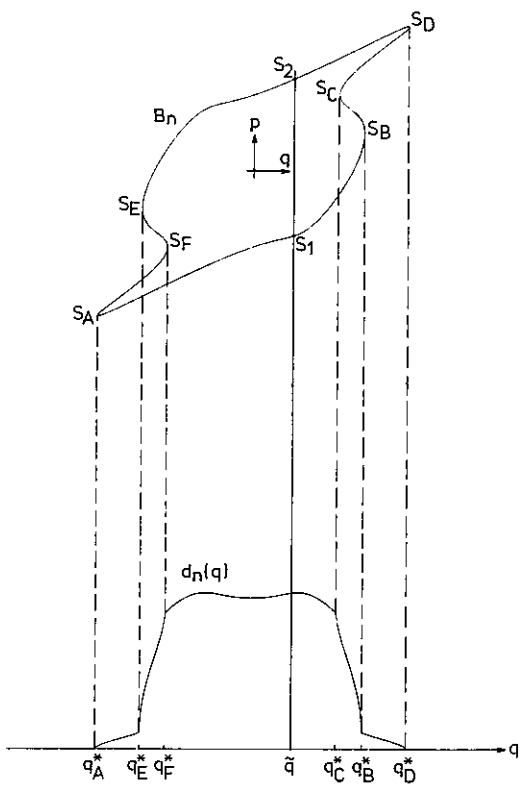

Fig. 2. A boundary curve B_n and the corresponding particle density $d_n(q)$ with anti-caustics at q^*.

3. Short- and long-range interactions

Let

$$U(q - q') \equiv u\left(\frac{q - q'}{L}\right), \tag{3.1}$$

where the length L is a measure of the range of the interaction.

For short-range interactions L is small in comparison with the dimensions of B. Significant contributions to the integral in (2.6) arise only from the points $s_1(\tilde{q}) \ldots s_m(\tilde{q})$, where m is the number of branches of B above $\tilde{q}$, defined as

$$\tilde{q} = q_n + p_n\,. \tag{3.2}$$

The $s_i(\tilde{q})$ are defined by

$$q(s_i(\tilde{q})) = \tilde{q}\,, \tag{3.3}$$

and illustrated in fig. 2 for a case where $m = 2$.

Expansion of the argument in U about s_i gives

$$\tilde{q} - q(s) = -(s - s_i)\cos\theta_i + \frac{(s - s_i)^2}{2R_i}\sin\theta_i\,, \tag{3.4}$$

where R_i is the radius of curvature of B at s_i. Substitution into (2.6) and use of (3.1) then leads to

$$p_{n+1} = p_n + 2\rho_0 L \sum_{i=1}^{m(\tilde{q})} \sin\theta_i \times \int_0^\infty \frac{\mathrm{d}Z u(Z)}{\sqrt{\cos^2\theta_i - \dfrac{2LZ\sin\theta_i}{R_i}}}\,. \tag{3.5}$$

Remembering that L is small, it is clear that the largest momentum kicks occurs near the anti-caustics (2.7) (see fig. 2). Thus for these nonlocal maps with short-range interactions and sharply-varying densities, anticaustics play an important role and lead to striking morphologies which do not occur in analogous point maps. In the limit,

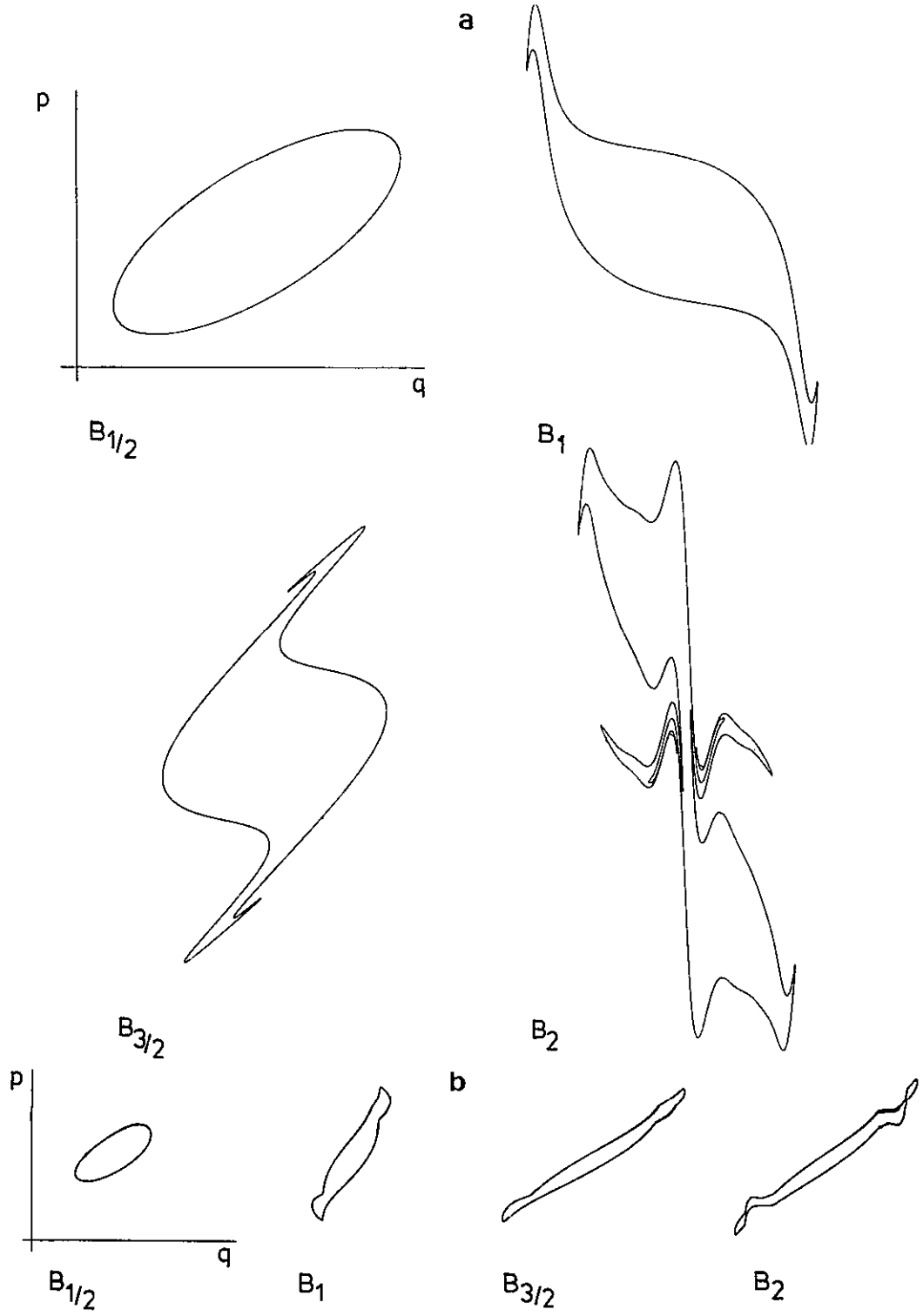

Fig. 3. The iterates $B_{1/2}$, B_1, $B_{3/2}$ and B_2 of a unit circle B_0. a) attractive short-range Gaussian interaction potential (8.1) with $A = 0.01$ and $C = -1.0$; b) repulsive short-range square-barrier potential (6.1) with $\epsilon = 1.0$ and $\Delta = 0.4$.

setting $L = 0$ in the square root in (3.5) would give

$$p_{n+1} = p_0 + \rho_0 \sum_{i=1}^{m(\bar{q})} \frac{\sin\theta_i}{|\cos\theta_i|} 2\int_0^\infty \mathrm{d}x U(x), \tag{3.6}$$

thus predicting infinite kicks at anticaustics for δ-function potentials.

The first morphologies arising on this basis for a short-ranged potential are illustrated in fig. 3 for the first few iterations of a simple B, computed exactly. Note how different is the behaviour for attractive and repulsive potentials. The importance of anticaustics for short-range interactions will be further illustrated in sections 6 and 8.

For long-range interactions, L is large in comparison with the dimensions of B. Then (3.1) can be expanded as follows (bearing in mind that U is an even function):

$$U(q-q') = u(0) + \frac{1}{2}\frac{(q-q')^2}{L^2}u''(0) + \frac{1}{24}\frac{(q-q')^4}{L^4}u''''(0) + \cdots, \tag{3.7}$$

When substituted into (2.2) this gives the momentum kick in terms of the *moments* of q over the density ρ, i.e.

$$\langle q^l\rangle \equiv \frac{1}{N}\iint \mathrm{d}q\,\mathrm{d}p\, q^l\rho(q,p) \quad (q,p\in B) = \frac{1}{N}\int \mathrm{d}q\, q^l\,\mathrm{d}(q). \tag{3.8}$$

Note that $\langle q\rangle = 0$ for the curves B we are considering, whose centre of mass remains at the origin. The resulting kick is

$$p_{n+1} - p_n = -\frac{N}{L^2}q_{n+1}u''(0) + \frac{N}{6L^4}u''''(0) \times (+\langle q^3\rangle - 3q_{n+1}\langle q^2\rangle - q_{n+1}^3) + \cdots. \tag{3.9}$$

A special case of this formula will be studied in section 7 which deals with the quartic potential.

This shows in a most transparent way the nonlocality of the map, which is embodied in the (global) moments $\langle q^l\rangle$, acting as coefficients (which change with time) of the terms in a polynomial point map. We shall later illustrate the effects of these coefficients in simple examples of quadratic and quartic potentials.

4. Quadratic potentials

The simplest non-trivial smooth potential is

$$U(q-q') = \frac{A}{2}(q-q')^2. \tag{4.1}$$

For this special case all properties of the map (4.1) can be discussed analytically. It follows immediately from (4.1) (or as a special case of the 'long-range' formula (3.9)) that

$$\begin{aligned} q_{n+1} &= q_n + p_n, \\ p_{n+1} &= -\gamma q_n + (1-\gamma)p_n, \end{aligned} \tag{4.2}$$

where

$$\gamma \equiv AN. \tag{4.3}$$

This is a local and linear map, with constant coefficients because N remains constant. Moreover, the form of the map is independent of the initial density $\rho_0(q,p)$.

The properties of linear point maps are well known [3, 9] and we just summarise them here. Let

$$M \equiv \begin{pmatrix} 1 & 1 \\ -\gamma & 1-\gamma \end{pmatrix}. \tag{4.4}$$

The map is *elliptic* if $|\mathrm{Tr}\, M| < 2$, i.e. $0 < \gamma < 4$, and *hyperbolic* if $|\mathrm{Tr}\, M| > 2$, i.e. $\gamma < 0$ or $\gamma > 4$.

In the elliptic case, there exist invariant densities ρ whose contours are concentric ellipses whose orientation and eccentricity depend on γ. Densities

ρ whose contours are ellipses different from the invariant ones will evolve quasiperiodically by changing their orientation and eccentricity (rotating and breathing) (the evolution is exactly periodic if the rotation number $(1/\pi)\arccos(1-\gamma/2)$ is rational).

In the hyperbolic case, the invariant densities have infinitely-extended hyperbolic contours, and as $n\to\infty$ initially-localized densities will stretch along an asymptote, whose equation is

$$p = q\left(\frac{\gamma\, e^{\phi}}{|\gamma|} - 1\right),$$

where (4.5)

$$\phi > 0 \quad \text{and} \quad \cosh\phi = |1-\gamma/2|\,.$$

5. Constant-force interactions

Consider the potential

$$U(q-q') = A|q-q'|\,, \tag{5.1}$$

which describes a constant force between the particles (one-dimensional electrostatics), attractive if $A>0$. It follows directly from (1.4) that the momentum kick for this case is

$$p_{n+1} - p_n = -A(N_L(q_{n+1}) - N_R(q_{n+1}))\,, \tag{5.2}$$

where N_L and N_R denote the number of particles to the left and right of q_{n+1} in the density immediately before the kick. Of course

$$N_L(q_{n+1}) + N_R(q_{n+1}) = N\,. \tag{5.3}$$

For a step-function density,

$$N_L(q) = \int_{q_L}^{q} dq' \int dp'\,, \quad (q', p' \in B_{n+1/2})\,,$$
$$N_R(q) = \int_{q}^{q_R} dq' \int dp'\,, \quad (q', p' \in B_{n+1/2})\,, \tag{5.4}$$

where q_L and q_R are the left and right extremes of $B_{n+1/2}$. The behaviour of $N_L(q) - N_R(q)$ for a simple closed curve symmetric with respect to the origin is illustrated in fig. 4. The function is odd, and approaches its extreme values as $(q-q_L)^{3/2}$ and $(q_R-q)^{3/2}$.

When combined with the q-shear, this form of momentum kick generates anti-clockwise-curling whorls if $A>0$ (in fig. 5), and persistent extension of B if $A<0$ (as might be predicted on physical grounds for this repulsive case).

A point map which behaves in a qualitatively similar fashion is that generated by the external potential $A|q|^{\alpha}$ where $1<\alpha<2$. We remark that a point map with the external potential (5.1) would lead to rupture of B at its intersections with the p axis, because the force (which governs the momentum kick) is discontinuous at $q=0$; in the nonlocal map 1.4 this discontinuity is smoothed by the integration over q'.

6. Square-well potentials

These potentials have the form

$$U(q-q') = \begin{cases} \epsilon\,, & \text{if } |q-q'| < \Delta\,, \\ 0\,, & \text{otherwise}\,, \end{cases} \tag{6.1}$$

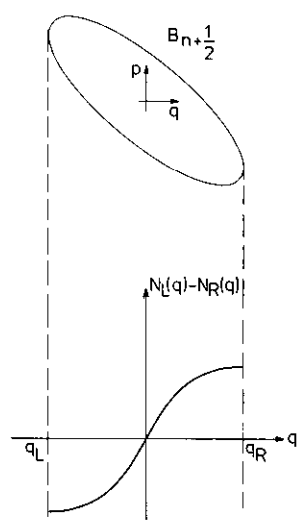

Fig. 4. A simple centrosymmetric curve and the behaviour of $N_L(q) - N_R(q)$ as defined by (5.4) for a step-function density.

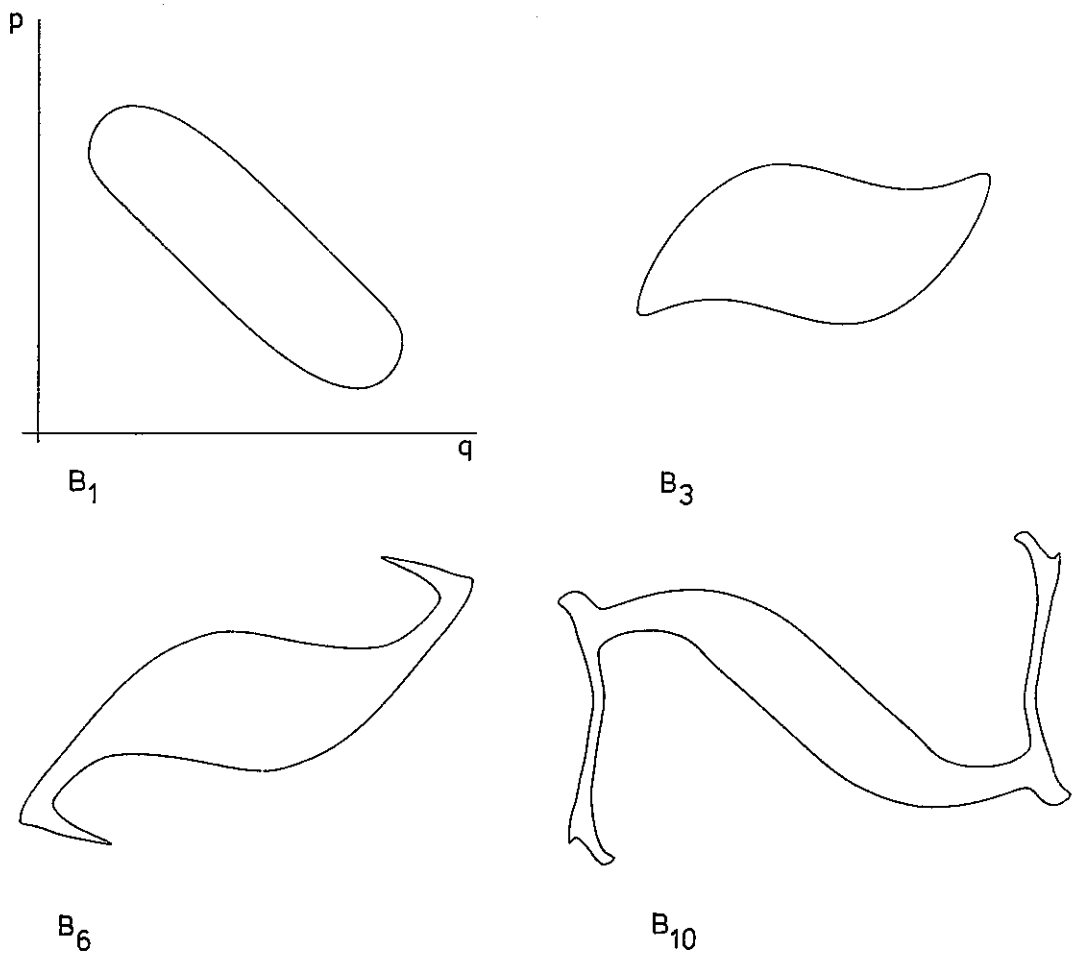

Fig. 5. The iterates B_1, B_3, B_6 and B_{10} of a unit circle B_0. The attractive constant-force interaction potential is given by (5.1) with $A = 0.5$.

where ϵ is the height and Δ the half-width. From (2.2) the momentum kick takes the particularly appealing form

$$\begin{aligned} p_{n+1} - p_n = &-\epsilon\rho_0 \iint \mathrm{d}q'\,\mathrm{d}p' \\ &\times \{-\delta(q_{n+1} - q' - \Delta) \\ &+ \delta(q_{n+1} - q' + \Delta)\} \\ = &\epsilon\{d_{n+1}(q_{n+1} - \Delta) - d_{n+1}(q_{n+1} + \Delta)\}\,. \end{aligned} \tag{6.2}$$

Thus the change in momentum is proportional to the difference in particle densities at a distance Δ to the left and right of q_{n+1}.

The momentum kick is a continuous function of q $(=q_{n+1})$ but has a discontinuous derivative at q values distant Δ from an anticaustic of B $(=B_{n+1/2})$. To see this, consider the case where B is the unit circle (fig. 6). Then $d(q+\Delta)$, which is proportional to the momentum chord-length at $q+\Delta$, is

$$d(q+\Delta) = 2\rho_0\,\mathrm{Re}(1-(q+\Delta)^2)^{1/2}\,, \tag{6.3}$$

whose derivative indeed diverges if $q+\Delta = \pm 1$. In general, $q-\Delta$ will not lie on an anti-caustic when

$q + \Delta$ does, and vice versa, so that there is no possibility of the singularities cancelling. As a result the boundary B will become decorated with *corners*. Fig. 7 illustrates this with the first few iterations of the unit circle (taken to be $B_{1/2}$) under the square-well map with parameters $\epsilon = -1$ and $\Delta = 0.4$.

For a smooth B_0 the first corners arise from the anticaustics and at birth possess one tangent which has infinite slope. In subsequent iterations, however, each corner not only shears but generates new ones, because no matter how it is oriented it will cause $d(q + \Delta) - d(q - \Delta)$ to have a discontinuous derivative when $q \pm \Delta$ lies on it; these new corners need not have an infinite slope. Therefore corners will proliferate and a rough estimate of their number after n iterations can be obtained as follows. If B_0 has two branches and hence two anti-caustics, B will have four corners. These will be sheared away from each other on $B_{3/2}$ and will produce sixteen new corners in B_2. Neglecting the generation of new anti-caustics and the resulting hierarchy of new corners, which will amplify the proliferation, we already have an exponential growth proportional to 5^n.

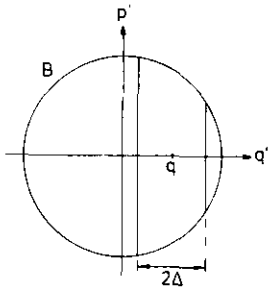

Fig. 6. Momentum chord-lengths at $q \pm \Delta$ inside a circle B.

If the mapping shown in fig. 7 is iterated further, and displayed together with the corresponding particle densities $d_n(q)$ (fig. 8), it becomes clear that, as well as growing more complicated, B is splitting into parts – the particle density is undergoing *fission*. This is a curious phenomenon for this case of an attractive interaction.

Fission is by no means a general phenomenon. For example if we start with a unit circle for B_0 (rather than $B_{1/2}$), then, as fig. 9 shows, great complexity develops, but not fission. The evolution of complexity is sensitive to the square-well parameters as well as the form of B_0, as is demonstrated in fig. 10 which has the same conditions as fig. 9 except that $\Delta = 1$ rather than 0.4. If Δ is increased further, to make the well-width appreciably larger than the size of B_0, the particles all remain for a while within each others wells and no interaction occurs for the first few iterations; this is illustrated in fig. 11 (for $\epsilon = -1.5$, $\Delta = 3.0$).

For repulsive potentials (square barriers) the evolution is less complicated. Typically, a simple B_0 is sheared into a long thin fibre decorated with small corners. Such behaviour is shown in fig. 3 (for $\epsilon = 1$, $\Delta = 0.4$).

Although the square well potential is inap-

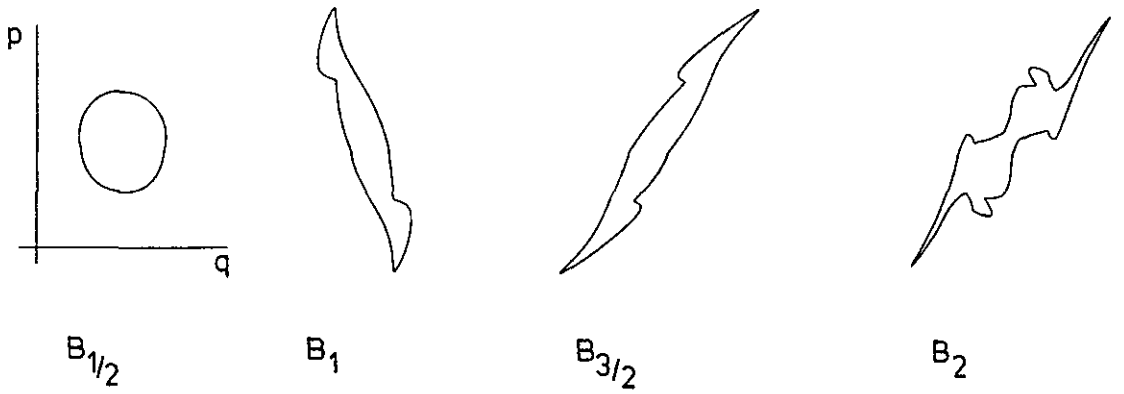

Fig. 7. The iterates $B_{1/2}$, B_1, $B_{3/2}$ and B_2 of an ellipse B_0 chosen such that $B_{1/2}$ is a unit circle. The attractive square-well interaction is given by (6.1) with $\epsilon = -1.0$ and $\Delta = 0.4$. The p kick on $B_{1/2}$ produces corners on B_1 at a distance Δ from anti-caustics.

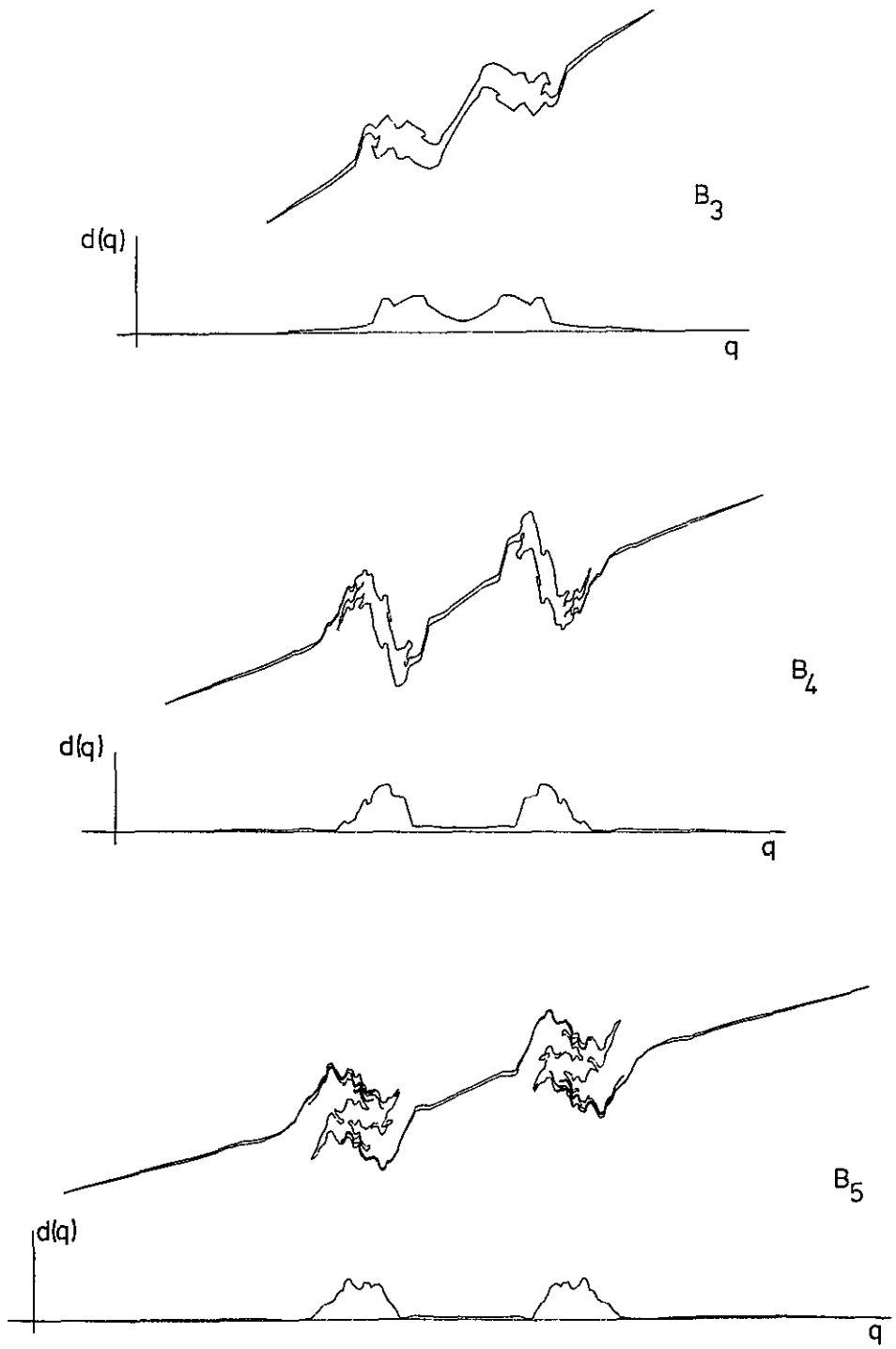

Fig. 8. The further iterates B_3, B_4 and B_5 of the curves in fig. 7, together with their particle densities $d(q)$, illustrating fission.

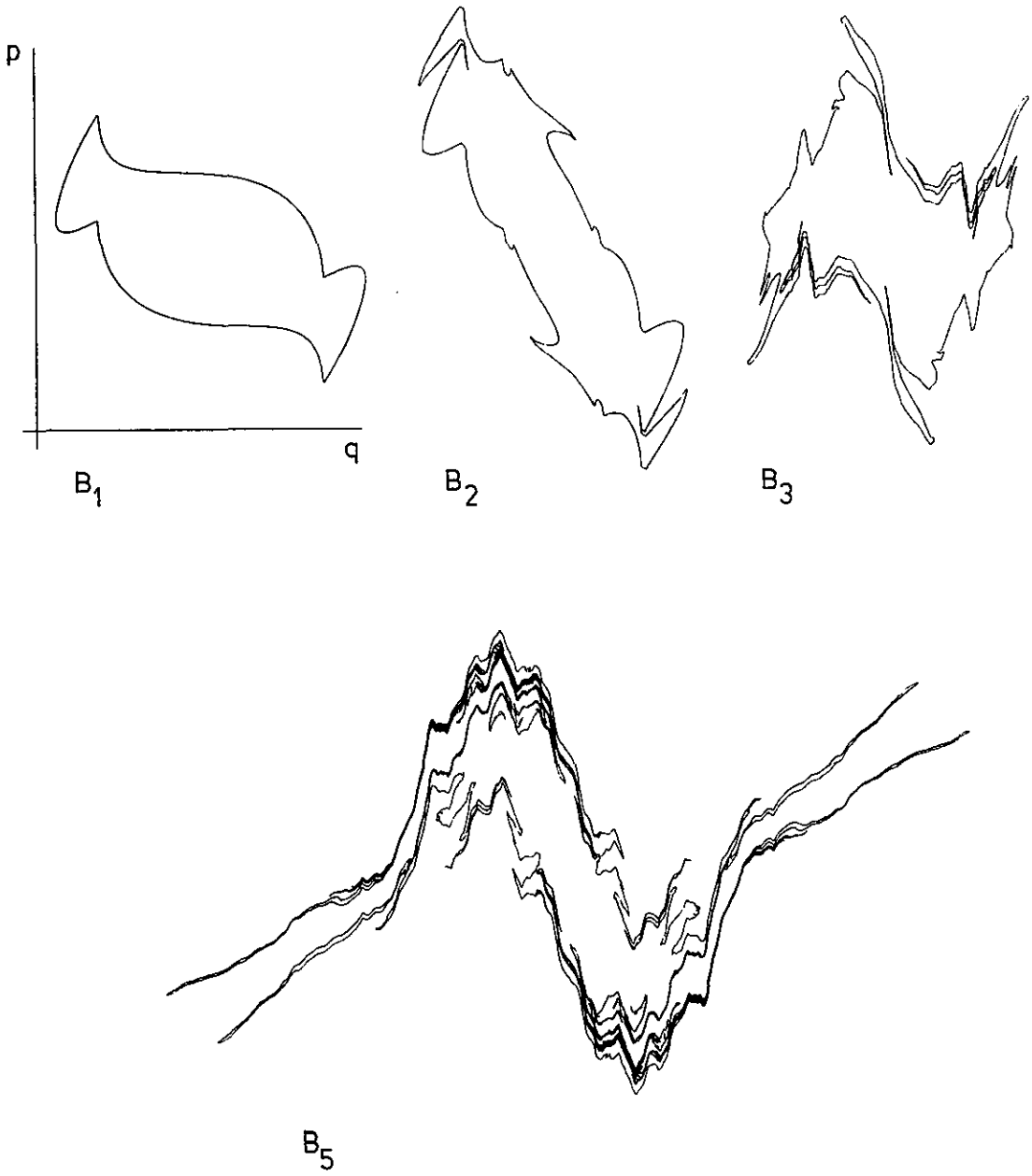

Fig. 9. The iterates B_1, B_2, B_3 and B_5 of a unit circle B_0. The attractive square-well potential is given by (6.1) with $\epsilon = -1.0$ and $\Delta = 0.4$.

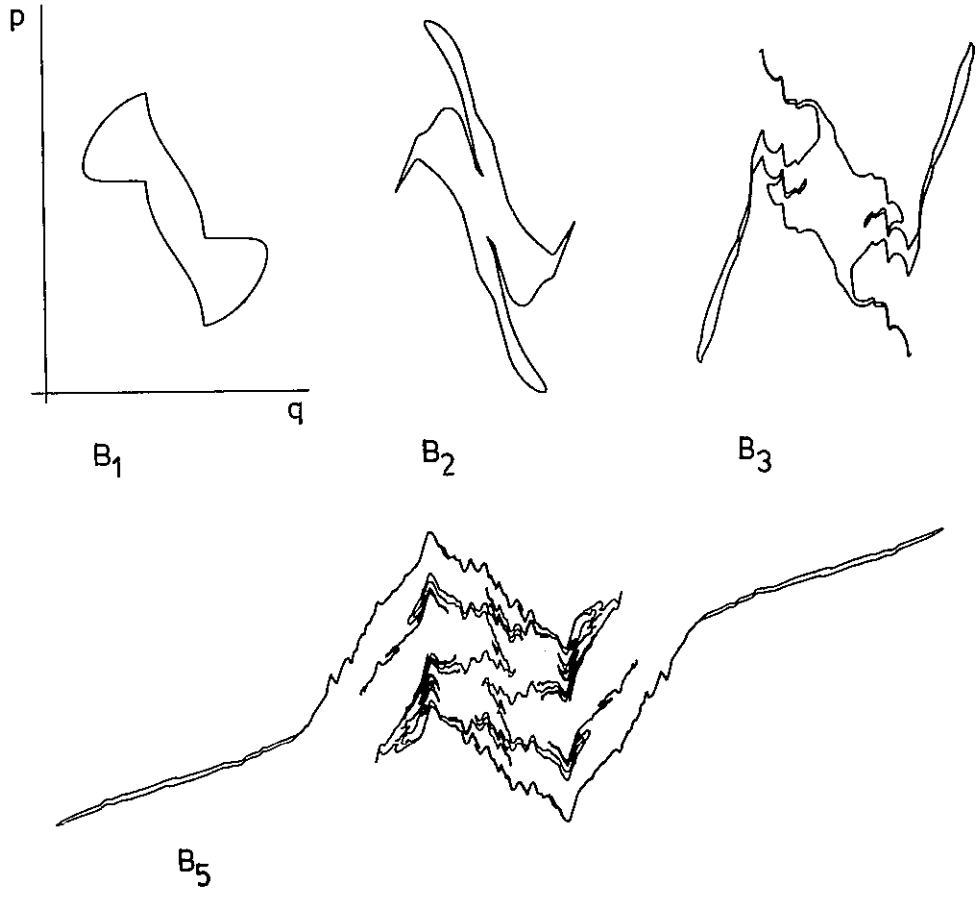

Fig. 10. As fig. 9 but with $\Delta = 1.0$.

propriate in a point map (because points at $q = \pm\Delta$ would receive infinite momentum kicks), it is possible to generate corners in point maps of curves by choosing potentials whose second derivative U'' is discontinuous at one or more points q^*; the corners are born at the points on B with coordinates q^*, and are subsequently sheared away from these positions.

7. Quartic potentials

$$U(q-q') = \frac{A}{2}(q-q')^2 + \frac{C}{4}(q-q')^4 . \tag{7.1}$$

The momentum kick is a special case of (3.9) which was derived for long-range potentials. We shall confine ourselves to boundaries B which are centrosymmetric (and trivially remain so under the map). Then (cf. (3.8)) $\langle q^3 \rangle = 0$ and (3.9) becomes

$$p_{n+1} - p_n = -Nq_{n+1}(A + 3\langle q^2 \rangle C) - NCq_{n+1}^3 . \tag{7.2}$$

It is convenient to rescale q and p and reduce the nonlocal map to the following maximally simple form:

$$\begin{aligned} Q_{n+1} &= Q_n + P_n , \\ P_{n+1} &= P_n - Q_{n+1}^3 - NQ_{n+1}\left(A + \frac{3\langle Q^2 \rangle}{N}\right) . \end{aligned} \tag{7.3}$$

Note that C has scaled away. This map is a perturbation of the quartic point map extensively

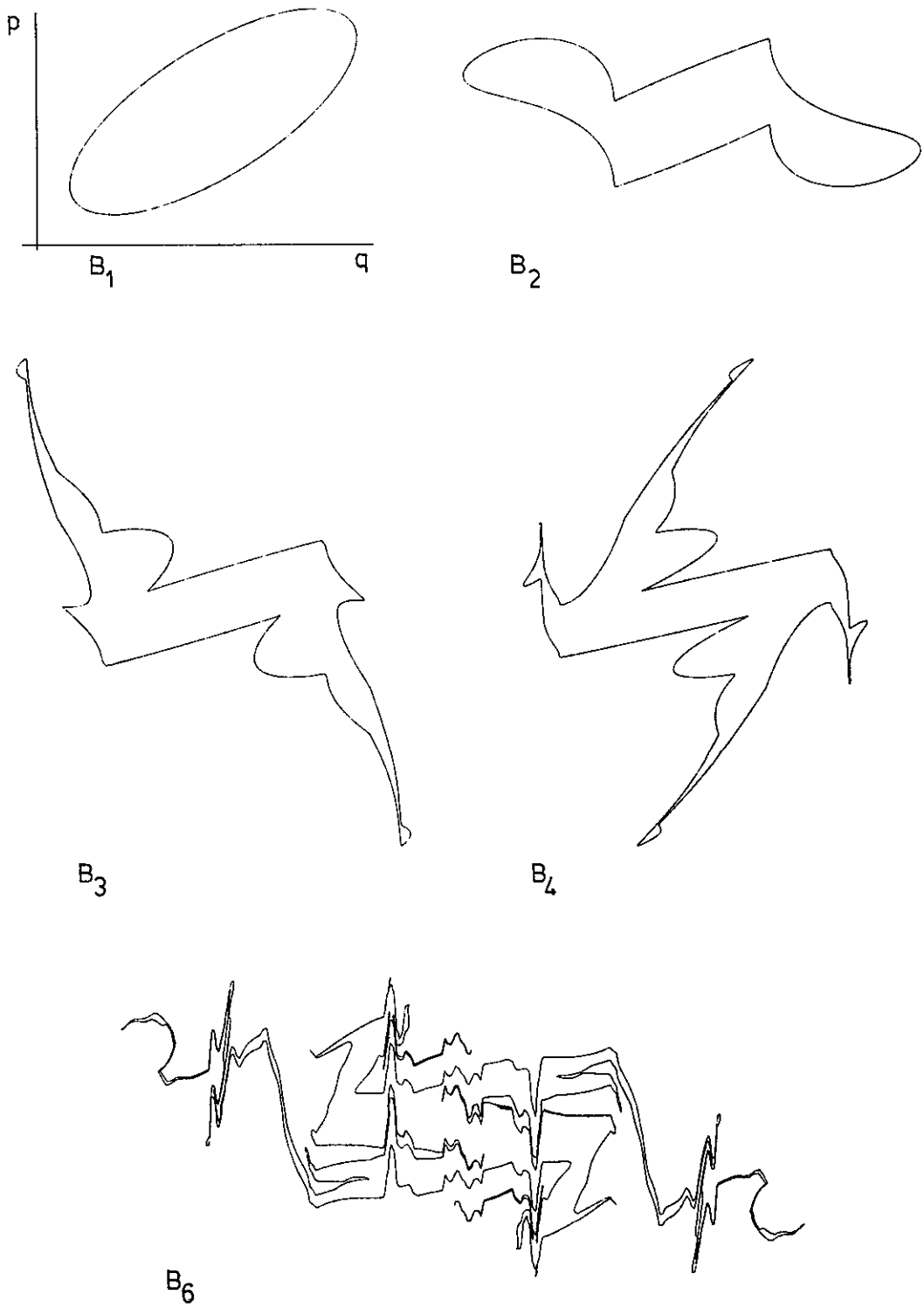

Fig. 11. The iterates B_1, B_2, B_3, B_4 and B_6 of a unit circle B_0. The attractive square-well interaction is given by (6.1) with $\epsilon = -1.5$ and $\Delta = 3.0$.

studied by Berry et al. [3, 5]. But the perturbation (the term linear in Q_{n+1} in the momentum kick) depends on the changing second moment $\langle Q^2 \rangle$ of $B_{n+1/2}$ and so incorporates the nonlocality. The principal effect of the time-dependent perturbation is to destroy the nontrivial elliptic and hyperbolic fixed points of the point map. Nevertheless, the evolution of curves generated by the nonlocal map is similar to that generated by the point map, because of the persistence of the elliptic fixed point at the origin and the chaotic region far from the origin. This can be seen by comparing fig. 12 (generated from the unit circle by (7.2) with $A = -0.08$, $C = 0.16$, $N = \pi$) with fig. 12a of [3]. It is of course possible that for some parameter values the two maps generate very different curves, but we have not found such a case in our numerical experiments.

8. Gaussian potentials

As a model for smoothly-varying interactions of finite range and which are entirely attractive or repulsive we choose

$$U(q - q') = \frac{C}{\sqrt{2\pi A}} e^{-(q-q')^2/2A} \tag{8.1}$$

and examine cases of short and medium range in order to make a comparison with the square-well morphologies of section 6.

First we follow the evolution under a deep narrow attractive Gaussian for which $A = 0.01$, $C = -1.0$ and whose half-width Δ (defined by $U(\Delta) = U(0)/e$) is about 0.15. The first few iterations were already presented in fig. 3a.

For a longer-range potential we choose again $C = -1.0$ but $A = 0.1$ so that $\Delta \simeq 0.4$. The evolution is shown in fig. 13 which should be compared with the corresponding square well curve maps in fig. 9. The greatest momentum kicks are received when q is a distance Δ from an anticaustic, but because U is smooth this does not generate corners. Although the curves B_2 are qualitatively similar in figs. 13 and 9, it is evident that the subsequent evolutions are very different. In particular, the Gaussian potential leads to fission

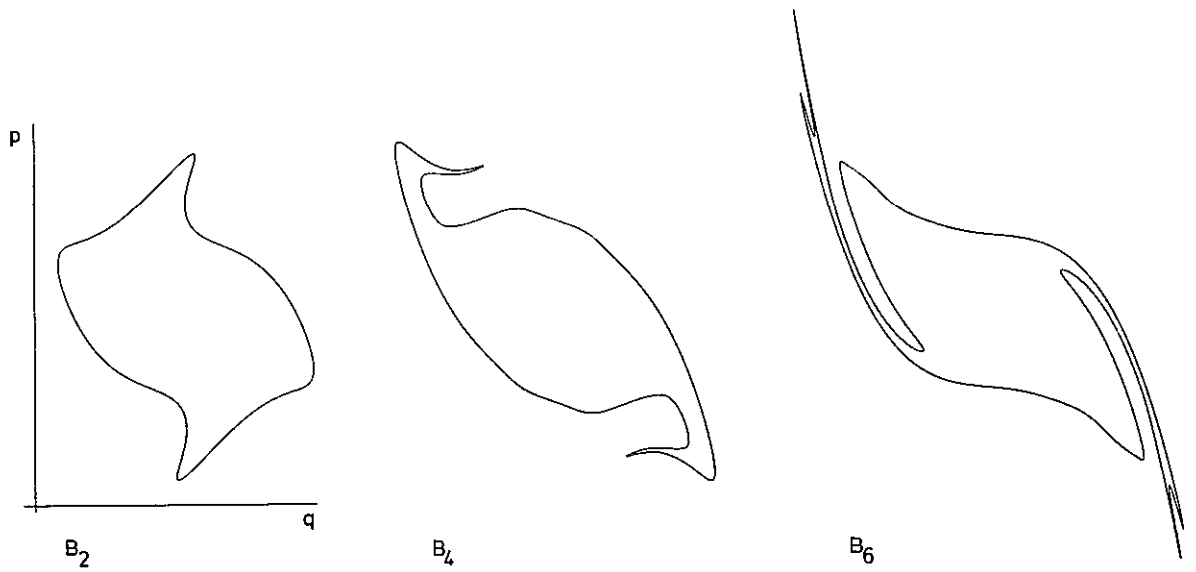

Fig. 12. The iterates B_2, B_4 and B_6 of a unit circle B_0. The attractive quartic potential is given by (7.1) with $A = -0.08$ and $C = 0.16$.

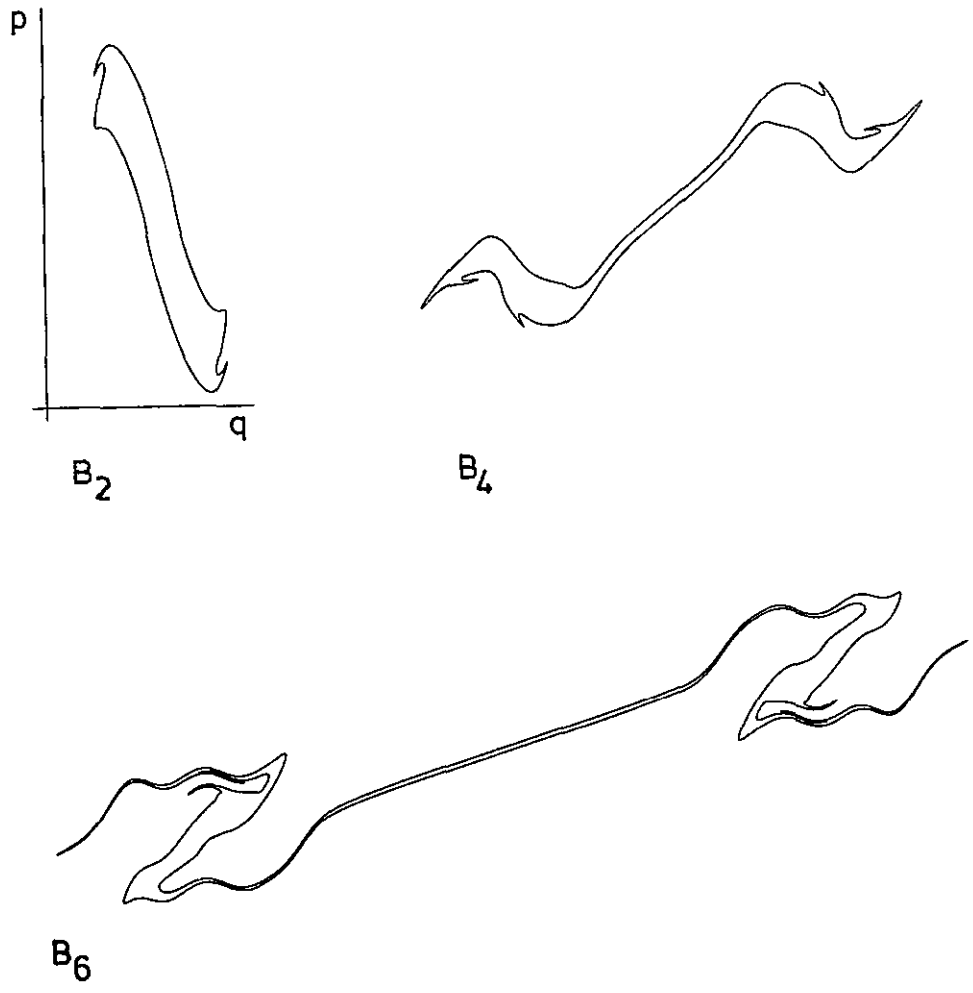

Fig. 13. The iterates B_2, B_4 and B_6 of a unit circle B_0. The attractive Gaussian potential is given by (8.1) with $A = 0.1$ and $C = -1.0$.

(B_6 in fig. 13) whereas no fission is evident in fig. 9. Note however that fission does occur in fig. 8, which was made in the same way as fig. 9 except that $B_{1/2}$, rather than B_0, was a circle.

For repulsive Gaussians no interesting morphologies were excepted or observed.

We remark here that in the case of point maps with Gaussian or similar potentials, curves (except those chosen to lie entirely between closed invariant curves) will not develop continuing complexity. Instead their branches will be most deformed near q-values where the force is greatest, and these deformations get sheared away into the force-free region and map away essentially unchanged. In the corresponding nonlocal maps, complexity growth is governed by the anticaustics, resulting in tendrilization on ever-finer scales in all regions of B.

9. Interatomic potentials

As a simple model for interactions in which the force does not have the same sign for all values of $q - q'$, we choose

$$U(q-q') = [A - C(q-q')^2]\exp\{-D(q-q')^2\}, \tag{9.1}$$

where all parameters are positive. We do not employ potentials of Lennard-Jones type, because their divergence at $q-q'$ (or indeed any divergence more severe than $(q-q')^{-1/2}$) would give rise to infinite momentum kicks at almost all q, and hence an immediate explosion of the particle density in the next period of free motion.

Fig. 14 shows a computer experiment with parameters $A = 1.0$, $C = 15.0$ and $D = 5.0$ (so that the potential passes through zero at $|q-q'| = \sqrt{A/C} \approx 0.25$ and has its minimum at $\sqrt{D^{-1} + A/C} \approx 0.5$), B_0 being the unit circle. The different signs of momentum kick corresponding to particles dominated by the attractive and repulsive regions of the potential are clearly evident in B_1. The fact that the potential becomes effectively more short-ranged as the iterations proceed and B stretches means that the anticaustics again domi-

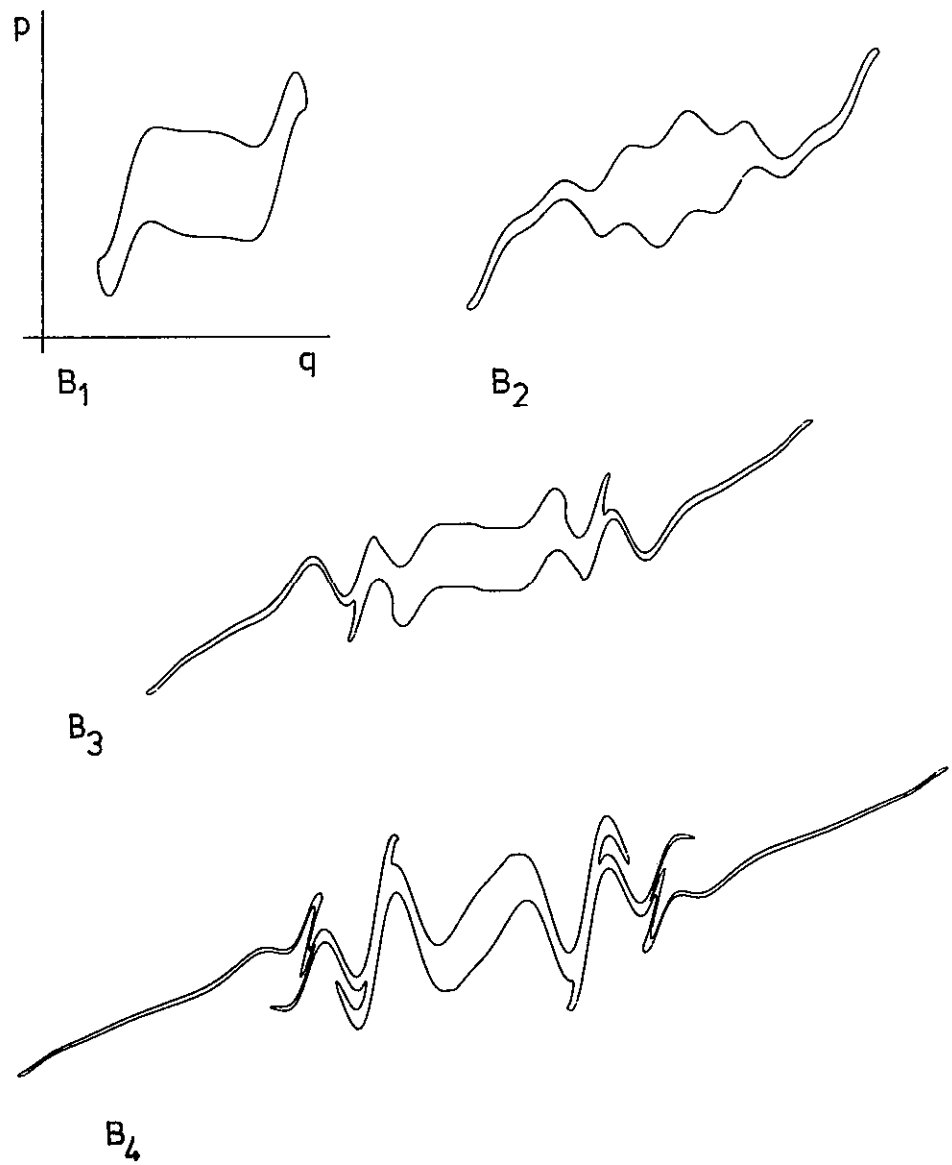

Fig. 14. The iterates B_1, B_2, B_3 and B_4 of a unit circle B_0. The interatomic potential is given by (9.1) with $A = 1.0$, $C = 15.0$ and $D = 5.0$.

nate and lead to increasing complexity. Some evidence of the coexisting attraction and repulsion persists in the alternating structure of B_4.

We also studied on the computer a case where A and C were negative, corresponding to short-range attraction and long-range repulsion. This gave rise to fission of the particle density into three parts – behaviour to be expected as the outer regions of B_0 are blown away by the repulsion to later cohere by near-neighbour attraction, along with the remaining central region of B_0.

10. Sinusoidal potentials

The periodic potential

$$U(q-q') = A\cos\{C(q-q')\} \tag{10.1}$$

leads on expanding the cosine to a nonlocal map with momentum kick

$$p_{n+1} - p_n = CNA\sin(Cq_{n+1})\langle\cos q\rangle - \langle CNA\cos(Cq_{n+1})\langle\sin q\rangle\,, \tag{10.2}$$

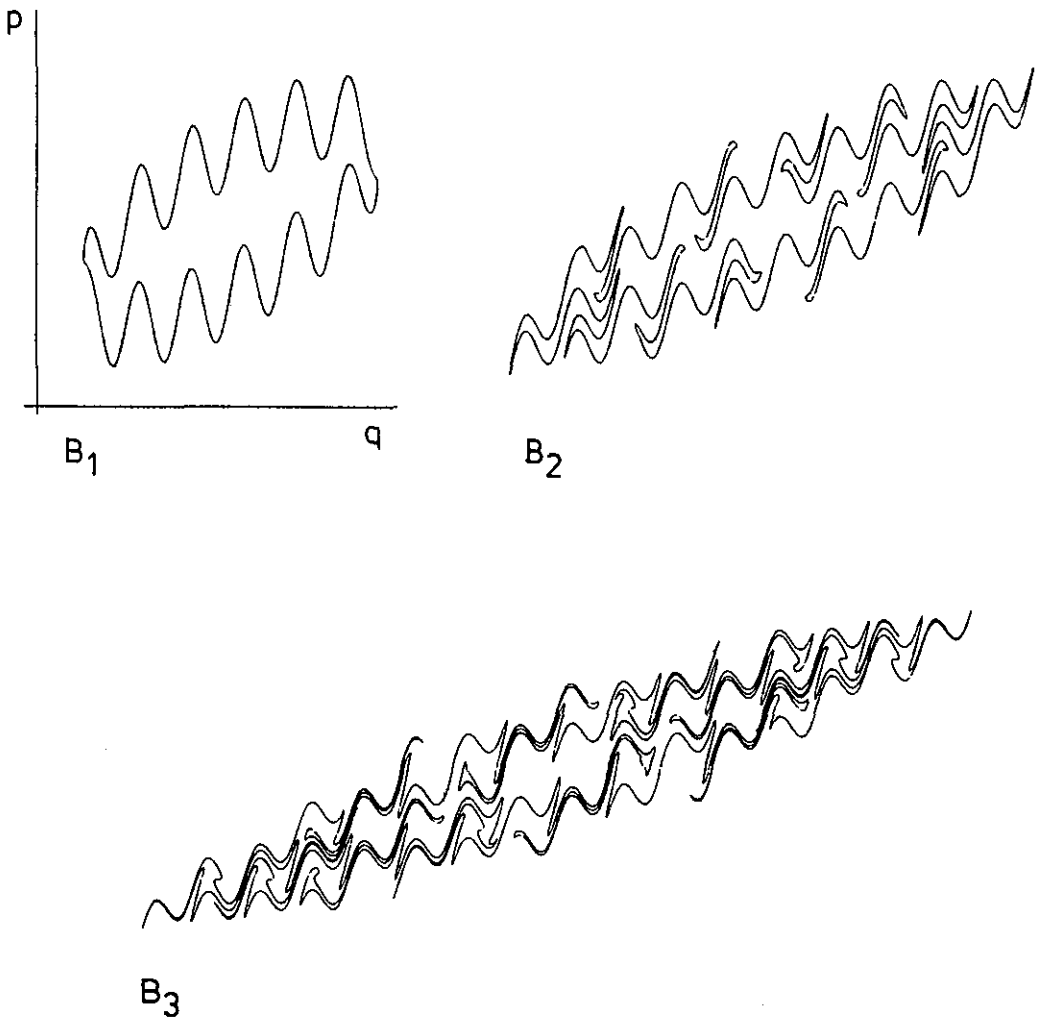

Fig. 15. The iterates B_1, B_2 and B_3 of a unit circle B_0. The sinusoidal potential is given by (10.1) with $A = -0.5$ and $C = 4\pi$.

where $\langle\ \rangle$ denotes moments over $B_{n+1/2}$ defined by analogy with (3.8). Once again we have a point map at each iteration with nonlocality embodied in coefficients that change with each iteration (cf. section 7).

For centrosymmetric B, $\langle \sin q \rangle = 0$ and the momentum kick (10.2) factorizes. The extrema and zeros of the momentum kick occur at the same q-values for all times. We can show that (10.1) is the only periodic potential with this property.

As fig. 15 shows (for $A = -0.5$, $C = 4\pi$ and the unit circle for B_0) this gives rise to complicated many-branched curves which however always display the periodicity of the potential. The behaviour is very similar to that generated by the analogous point map, in spite of the changing value of $\langle \cos q \rangle$.

In this context of periodic potentials it would be appropriate to study the evolution not just of closed curves B, representing normalized densities $\rho(q,p)$ or $d(q)$, but non-bounded curves corresponding to periodic densities (such as charge density waves). Interesting effects can be expected to depend on the commensurability of the period of B_0 with respect to that of the interaction, but we have not investigated these possibilities.

11. Fusion

This section is a brief description of a numerical experiment in which B_0 consisted of two separate closed curves ('blobs'), corresponding to two spatially separated particle densities. The interaction between particles (irrespective of which blob they belong to) was the attractive Gaussian (8.1) with $A = 0.1$ and $C = -1.0$.

As fig. 16 shows, the interpenetration of the separate curves soon becomes so intimate that it is difficult to identify them, and it is sensible to speak of a fusion of the particle densities, even though the curves maintain their topological identities. Of course the phenomena fusion and fission are complementary because of the symmetry of the maps under time reversal.

Fig. 17 is the same as fig. 16, except that the form of B_0 is different. Nevertheless the evolution is very different. B_4 consists of two curves one on top of the other, which hardly interpenetrate (although their particle densities $d(q)\,\mathrm{d}o$). This illustrates the sensitivity of nonlocal interactions to initial conditions, previously noted for fluid vorticity by Zabusky [7]. Fusion of fluid vorticity distributions was studied by Overman and Zabusky [11].

12. Energy and integrability

The energy of a single particle in the state q, p at time t is

$$\mathscr{H}(q,p,t) = \frac{p^2}{2m} + \int\int \mathrm{d}q'\,\mathrm{d}p' V(q-q',t) \times \rho(q',p',t), \tag{12.1}$$

where V is the (impulsive) potential energy,

$$V(q-q',t) = TU(q-q') \sum_{n=-\infty}^{\infty} \delta(t-nT). \tag{12.2}$$

In field-theory language, $\mathscr{H}$ is a Hamiltonian density determining the field ρ by Hamilton's equations and the continuity equation which together give

$$\frac{\mathrm{d}\rho}{\mathrm{d}t} = \frac{\partial\rho}{\partial t} + \{\rho, \mathscr{H}\} = 0 \tag{12.3}$$

and from which in turn the nonlocal map (1.4) can be obtained.

The total energy of the assembly of particles (i.e. of the field) is

$$E(t) = \int\int \mathrm{d}q\,\mathrm{d}p \frac{p^2}{2m}\rho(q,p,t) + \tfrac{1}{2}\int\int\int\int \mathrm{d}q\,\mathrm{d}p\,\mathrm{d}q'\,\mathrm{d}p' \times V(q-q',t)\rho(q',p',t)\rho(q,p,t). \tag{12.4}$$

Note that E is not simply the integral of $\rho\mathscr{H}$

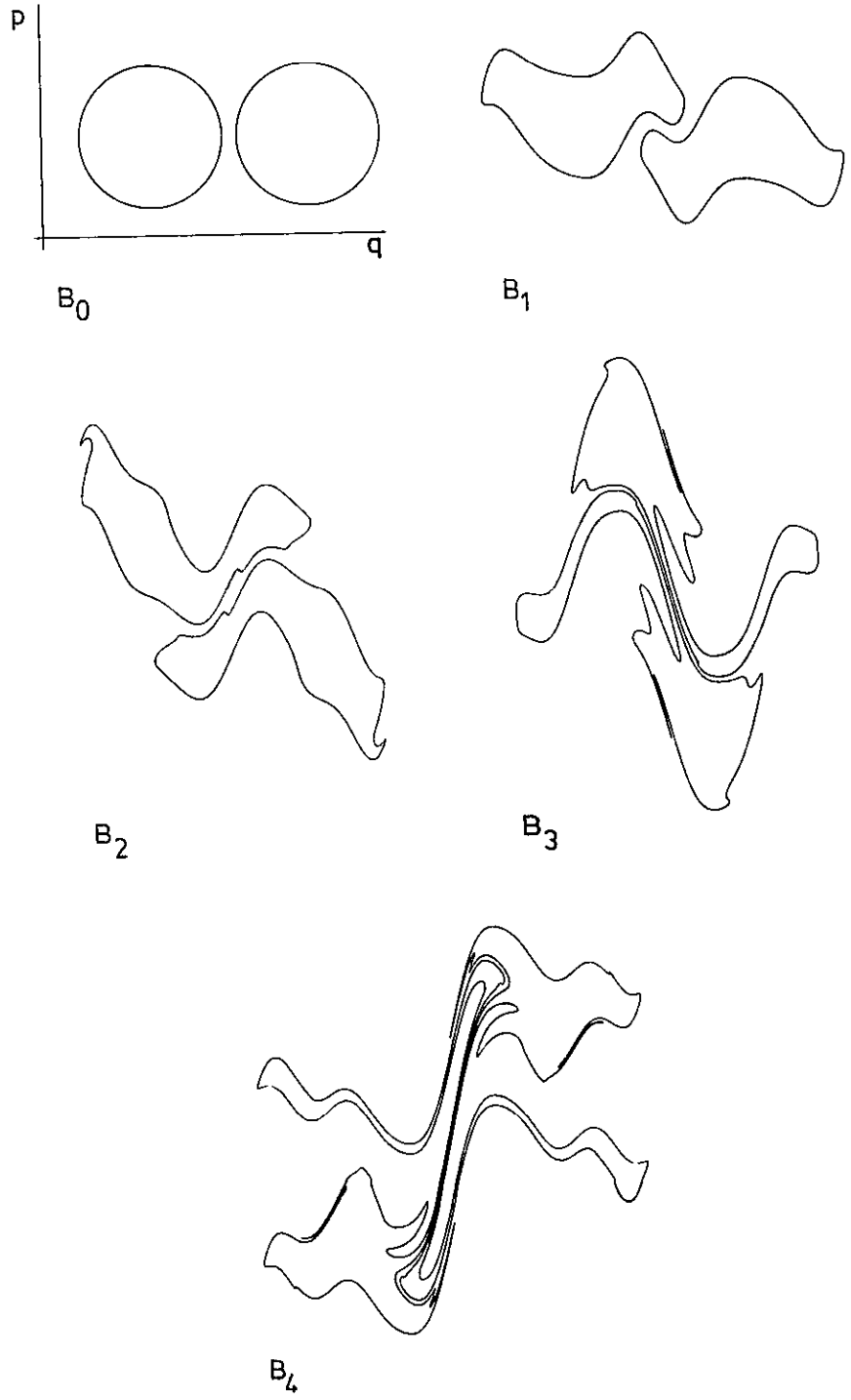

Fig. 16. The curve B_0 consisting of two unit circles, and its iterates B_1, B_2, B_3 and B_4, illustrating fusion. The attractive Gaussian potential is given by (8.1) with $A = 0.1$ and $C = -1.0$.

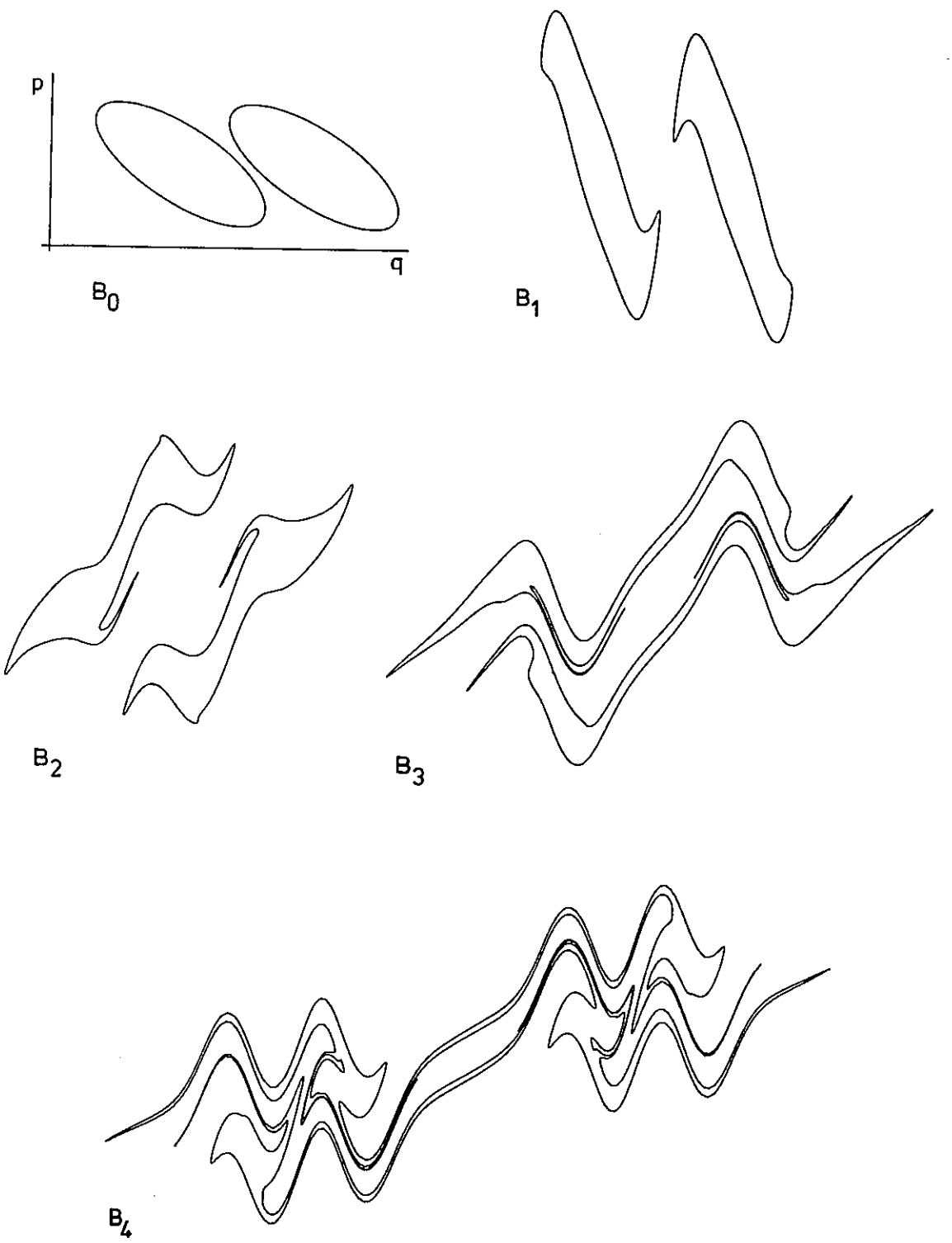

Fig. 17. As fig. 16 except that B_0 consists of two ellipses, chosen such that $B_{1/2}$ consists of two unit circles.

because of the factor $\frac{1}{2}$ necessary to avoid counting interactions twice.

In general neither $\mathscr{H}(q, p, t)$ along the trajectory of a phase point nor $E(t)$ is conserved. $\mathscr{H}$ changes not only because the interaction V is being switched on and off but also because each point moves in the changing environment of all the others. E changes because of the switching off of V, which in physical terms would require the particles to possess further freedoms (not explicitly considered here) providing the sources of the potential energy between particles (for example clocks controlling the current through resistive spring couplings whose stiffness is temperature dependent). An easy way to see that E must change is to compare the situations immediately following successive kicks, when the energy is all kinetic: after the first kick the particles all move freely and the kinetic energy remains the same, but at the second kick the momenta change and consequently the kinetic energy changes.

In the continuous-time limit $T \to 0$, V in (12.2) can be replaced by its time-average value $U(q - q')$. The particle energy $\mathscr{H}$ is still not conserved because of the time-dependence of ρ in (12.1), i.e. because of the changing environment. But now the total energy E is conserved, as is obvious physically and can be verified by a careful calculation (which holds also for the more general interaction potential $U(q, p; q', p')$ provided this is symmetric under exchange of q, p with q', p' as it must be for identical particles).

For the discrete-time case, it is possible to calculate what might be called the 'pseudo-energy', by replacing $V(q - q', t)$ by $U(q - q')$ in (12.4), i.e. the energy that the actual non-locally-mapping ρ would have in the time-average interaction. There is of course no reason to expect the pseudo-energy to be conserved, and it is not. We have computed the evolution of the pseudoenergy for square well potentials and observed that for attractive interactions it typically oscillates with a period of a few time steps, the oscillations getting weaker after fission in cases where this occurs (for repulsive forces, the pseudoenergy tends monotonically to its asymptotic value corresponding to free motion). For quadratic potentials we have confirmed the nonconservation of pseudo-energy by direct analytical evaluation.

Now we come to a question we have avoided posing until now: are nonlocal maps integrable? The answer appears to be that they are not, although we cannot give a proof. Integrability in a field theory would require there to exist infinitely many conservation laws in the form of integrals over the phase plane, involving $\rho(q, p, t)$. We know only two: the particle number (1.1), and the total momentum $\int\int \mathrm{d}q\, \mathrm{d}p\, p\rho$ (whose conservation was responsible for keeping our boundaries B centered on the origin). In the continuous-time limit, the energy (12.4) is conserved but no other quantity seems to be, consistent with the fact (?) that the problem on N particles on a line has no analytic solution (except for special interactions).

13. Conclusions

It should be obvious that the research reported here is little more than a preliminary survey of what looks like a rich area of mathematical physics; much more work is needed. Computationally, more systematic and extensive explorations of different types of interaction U and initial distribution ρ_0 are required. More important, however, is the need for an analytical understanding based on theorems about nonlocal maps. In particular we know nothing in general about the existence or nature of 'eigen-distributions' which remain unchanged, or are periodic, under the map (these would be 'fixed points' of the field theory). And we know nothing about the nature of the complexity of evolving curves B_n in the asymptotic limit $n \to \infty$: are the curves fractal and if so what determines their Hausdorff dimension?

What we have demonstrated, in some cases analytically, is the inevitable development of ever-finer structures in B_n, sensitively-dependent on B_0. For short-range interactions the development complexity of B is governed by its anticaustics. The

finest scales of this structure might be smoothed away if ρ does not have the step-function form employed throughout most of this paper. For example, a semiclassical assembly of interacting Fermions at *nonzero* temperature will be described by a density in the form of a smoothed step. (Thus temperature will act to smooth away what would otherwise evolve into infinite complexity, as Planck's constant smooths the Wigner function in a quantum map [5], and viscosity smooths the convolutions of vorticity contours in plane flow [6, 7].)

Finally, we recall that for some interactions the nonlocal map was equivalent to a point map with n-dependent coefficients. It is an interesting question, to which we do not know the answer, whether the enormous freedom in the choice of B_0 (or even ρ_0) is sufficient to enable nonlocal maps to mimic point maps whose coefficients have *arbitrary* n-dependence.

Acknowledgements

M.V.B. and N.L.B. were supported in part by the U.S. National Science Foundation. J.O.I. is Research Assistant of the National Fund for Scientific Research, Belgium. M.T. was supported by La Jolla Institute and the U.S. Dept. of Energy contract DOE 1/10923.

Appendix A

Numerical and graphical precision

A.1. Linear versus quadratic algorithms

In studying the evolution of a boundary B under the nonlocal map (1.4), it is important to compute the phase–plane integral, or equivalently the integration along B as in (2.6), as efficiently as possible. Let M be the number of points which are joined by straight segments to draw B. In order to compute the iterate of B one must in principle carry out M^2 manipulations: for each of the M points, an integral along B, involving M operations, must be performed.

In many cases, however, it is possible to bring the number of steps down from M^2 to M. This simplification is apparent from the formulae (4.2) for quadratic (trivial), (5.2) for constant-force, (6.2) for square-well, (7.3) for quartic and (10.2) for sinusoidal potentials. In the nontrivial of these cases, one must either compute once for every timestep a global function of B (e.g. its q-variance), which takes M steps, or one must compute for every point along B chord-lengths or partial areas, which can be done in one step from efficiently stored coordinates of points on B.

As M is proportional to graphical precision we have, for many potentials, algorithms for which computation time increases only linearly with precision. This means that any desirable precision can be obtained with standard minicomputers – at least to the resolution of our pictures. These algorithms are not available for the Gaussian and interatomic potentials; for these, (2.6) was used directly, requiring M^2 steps per iteration.

A.2. Refuelling

Points on B which are close may be kicked far apart in one iteration because of the unpredictability connected with the non-integrability of the map. To preserve precision it is then necessary to insert extra points and keep the largest separation along B below a specified threshold. One might think of interpolation techniques for determining the positions of the extra points but the error is then uncontrollable because the real B may be complicated where points are separating rapidly.

We choose instead to perform a *recursive refuelling* of B. The idea is as follows. Consider a simple B_0, say a circle, consisting of M_0 connected points; typically, M_0 might be as small as 200. B_0 is mapped to $B_1 \ldots B_n$ until the separation between any neighbouring points x_i and x_{i+1} exceeds a tolerance ϵ. Then a few extra points are inserted, not on B_n, but at exact positions between x_i and x_{i+1} on B_0. The map is then restarted from the

refuelled B_0. In this way one economically achieves optimal graphical precision. For the most complicated curves the final M was between 2000 and 4000.

To close these remarks we indicate three tests of the accuracy of our computations: firstly, a numerical test of area-preservation (better than one part in 10^3 in all cases); secondly, a graphical test of phase–plane projections onto q and p (e.g. the projections $d(q)$ onto q must be the same for $B_{n+1/2}$ and B_{n+1}): and thirdly the most severe test of reversibility.

References

[1] M.V. Berry, in: Topics in Nonlinear Mechanics, S. Jorna, ed., Am. Inst. Phys. Conf. Proc. No. 46 (1978) 16–120.

[2] R.H.G. Helleman, in: Fundamental Problems of Statistical Mechanics, vol. V, E.G.D. Cohen, ed. (North-Holland, Amsterdam, 1980) pp. 165–233.

[3] M.V. Berry, N.L. Balazs, M. Tabor and A. Voros, Ann. Phys. N.Y. 122 (1979) 26–63.

[4] M.V. Berry and N.L. Balazs, J. Phys. A12 (1979) 625–42.

[5] H.J. Korsch and M.V. Berry, Physica 3D (1981) 627–636.

[6] N.J. Zabusky, M.H. Hughes and K.V. Roberts, J. Comput. Phys. 30 (1979) 96.

[7] N.J. Zabusky, in: Proc. Orbis Scientiae (Miami) on the significance of nonlinearity in the natural sciences. A. Perlmutter and L.F. Scott, eds. (Plenum, New York, 1977) pp. 145–205.

[8] M.V. Berry, J. Phys. A 10 (1977) 2083–91.

[9] I. Percival and D. Richards, Introduction to Dynamics (Cambridge Univ. Press, London, 1982).

[10] G.S. Deem and H.J. Zabusky, Phys. Rev. Lett. 40 (1978) 859–62.

[11] E.A. Overman II and N.J. Zabusky, Phys. Fluids 25 (1982) 1297–1305.